CAMBRIDGE
UNIVERSITY PRESS

Article

Marshallsussmanite, NaCaMnSi$_3$O$_8$(OH), a new pectolite-group mineral providing insight into hydrogen bonding in pyroxenoids**

Marcus J. Origlieri[1]*, Robert T. Downs[1], Derek R. Hoffman[1], Mihai N. Ducea[1,3] and Jeffrey E. Post[2]

[1]Department of Geosciences, University of Arizona, Tucson, Arizona 85721–0077, USA; [2]Department of Mineral Sciences, Smithsonian Institution, P.O. Box 37012, MRC 0119, Washington, D.C. 20013–7012, USA; and [3]Faculty of Geology and Geophysics, University of Bucharest, Bulevardul N. Bălcescu 1, Bucharest 030167, Romania

Abstract

Marshallsussmanite (IMA2013-067) is a new pyroxenoid mineral from the Wessels mine, Kalahari Manganese Field, Northern Cape Province, South Africa. Marshallsussmanite has ideal formula NaCaMnSi$_3$O$_8$(OH) and triclinic P$\bar{1}$ symmetry. Marshallsussmanite forms vitreous pink bladed crystals to 2.1 cm. The mineral shows perfect cleavage on both {100} and {001}. The chemical composition from electron microprobe (average of 20 analyses) and inductively coupled plasma mass spectrometer analysis (average of three analyses) is Li$_2$O 0.43, Na$_2$O 8.06, MgO 0.08, CaO 15.33, MnO 21.79, SiO$_2$ 51.71; totalling 97.40 wt.%. The empirical formula, normalized to 3 Si and assuming 1 H apfu is Li$_{0.100}$Na$_{0.906}$Ca$_{0.953}$Mg$_{0.007}$Mn$_{1.071}$Si$_3$O$_8$(OH). Unit-cell parameters from single crystal X-ray diffraction are a = 7.7854(4), b = 6.9374(4), c = 6.8516(3) Å, α = 90.683(3)°, β = 94.330(3)°, γ = 102.856(3)°, V = 359.59(3) Å^3; Z = 2. The crystal structure refinement converged with R_{obs} = 0.0248 and site occupancy refinement gives crystal chemistry [Na$_{0.948}$Li$_{0.052}$][Ca$_{0.793}$Mn$_{0.207}$][Mn$_{0.937}$Ca$_{0.063}$]Si$_3$O$_8$(OH). Marshallsussmanite is a single chain silicate with a repeat interval of three tetrahedra (i.e. *dreier* chain). Marshallsussmanite is a member of the pectolite group of pyroxenoids, which also includes barrydawsonite-(Y), cascandite, pectolite, serandite and tanohataite. Parallel silicate chains form layers, intercalated with well-ordered cation layers. Calcium and Mn both exhibit octahedral coordination, while Na has four bonded interactions in a coordination sphere (radius 3 Å) of seven separate O atoms. Procrystal electron density and bond valence modelling results are compared. The mineral has an unusually strong hydrogen bond with O4···O3 separation of 2.458(2) Å. Unlike pectolite and serandite, O4 in marshallsussmanite acts as an H-bond donor and O3 is an H-bond acceptor. Cation ordering in pyroxenoids has a substantial impact on the H position and corresponding H-bonding schemata.

Introduction

THE mineral now known as pectolite entered the mineralogical lexicon in the early nineteenth century, when von Kobell (1828) named 'Pektolith'. The original definition of 'Pektolith' was chemical, based upon its relative contents of water, silica, sodium and calcium, altogether distinct from already known species (i.e. mesolite, natrolite and apophyllite). The name 'Pektolith' (now pectolite) comes from the Greek πηκτοσ, 'well put together', in allusion to its typical formation as tightly packed acicular crystals (Chester, 1896; Hintze, 1897).

Certain later discoveries of pectolite showed anomalous contents of Mn, such as 'manganopektolith' described by Williams (1891), which contains 4.25 wt.% MnO and 30.28 wt.% CaO. Later, Winther (1901) described the species 'schizolite', optically similar to pectolite, but containing 12.90 wt.% MnO and 19.48 wt.% CaO. The mineral showed optical extinction parallel to the elongation of cleavage splinters, which is consistent with monoclinic symmetry. More than a century after the description of pectolite, Lacroix (1931) described 'sérandite', a pectolite-like sodium calcium manganese silicate from French Guinea with significant dominance of Mn over Ca, specifically 28.99 wt.% MnO and 10.42 wt.% CaO. In accord with previous studies, Lacroix (1931) also proposed monoclinic symmetry for serandite.

Standard references of the late nineteenth century (e.g. Dana, 1892; Hintze, 1897) reported monoclinic symmetry for pectolite. However, Warren and Biscoe (1931) observed triclinic symmetry

This new mineral was originally approved by IMA in CNMNC newsletter 18, published in 2013 (IMA2013-067, *Min. Mag.*, **77, 3256). Subsequent to prepublication on the journal's website, new information came to light and in May 2018 the CNMNC of the IMA passed memorandum IMA 18-B: Discreditation of the mineral name 'marshallsussmanite' with a reinstatement of the name schizolite (Newsletter 43, *Min. Mag.*, **82**, 785). An alternative paper was published by Grice *et al.* (2019). The original *Mineralogical Magazine* paper could not be withdrawn as it has already been cited. It is published here to complete the publication record. Readers' attention is directed to the updated paper (Grice *et al.*, 2019, *Min. Mag.*, **83**, 473–478).

in an early X-ray diffraction investigation of pectolite. Using the contemporarily favoured method of reflection goniometry, Peacock (1935) also affirmed triclinic symmetry.

Schaller (1955) reconciled the previous studies of pectolite, 'schizolite' and serandite. Noting similarities in powder X-ray diffraction patterns for these phases, Schaller (1955) inferred an isostructural relationship. Plotting the refractive indices *vs.* Ca/Mn ratio, Schaller (1955) demonstrated a linear variation of optical parameters of pectolite, 'schizolite' and serandite with composition, concluding that a continuous series existed between isostructural end-members pectolite, $NaCa_2Si_3O_8(OH)$ and serandite, $NaMn_2Si_3O_8(OH)$. Furthermore, Schaller (1955) also discredited 'schizolite' as Mn-bearing pectolite.

Buerger (1956) solved the crystal structure of pectolite, finding a single silicate chain with a repeat unit of three tetrahedra, and a double octahedral ribbon of edge sharing CaO_6 polyhedra. In a later refinement of pectolite, Prewitt (1967) located a H atom between O3 and O4 by examining difference-Fourier maps. Takéuchi *et al.* (1976) determined the crystal structure of isostructural serandite, and revealed ordering of Ca into the M1 site. Ohashi and Finger (1978) demonstrated ordering of Na, Ca and Mn into the A, M1 and M2 sites, respectively, within the pectolite–serandite crystal structure. The strong ordering preference for Na, Ca and Mn cations implied a possible ordered intermediate $NaCaMnSi_3O_8OH$ with the pectolite structure. Notably one of their samples, SCH ('schizolite'), shows dominance (64%) of the $NaCaMnSi_3O_8OH$ component and corresponds to the new mineral described herein.

Strong hydrogen bonding within the pectolite group has received much study (Prewitt, 1967; Takéuchi *et al.,* 1976; Takéuchi and Kudoh, 1977; Jacobsen *et al.,* 2000; Arakcheeva *et al.,* 2007; Williams and Weller, 2014). Prewitt (1967) noted the proximity of non-bridging O atoms in the silicate chain of pectolite, estimating an O3···O4 separation of only 2.482 Å. In the structure of serandite, Takéuchi *et al.* (1976) found a yet shorter O3···O4 separation of 2.453 Å. Prewitt (1967) and Arakcheeva *et al.* (2007) both located H closer to O3 than O4 in pectolite, indicating an asymmetric H bond. Using single-crystal neutron diffraction on serandite, Jacobsen *et al.* (2000) found an irregular feature in the difference map, which they modelled as two separate H positions. Like in pectolite, Jacobsen *et al.* (2000) found the bulk of the H atom occupancy nearer O3 in serandite (despite a split site model). Clearly, O3 and O4 have distinct bonding environments in pectolite-group minerals.

This study characterizes a natural occurrence of ordered $NaCaMnSi_3O_8(OH)$, herein naming this new species marshallsussmanite. The mineral and mineral name have both received approval from International Mineralogical Association (IMA2013-067). Type material is deposited in the collections of the University of Arizona Mineral Museum, Tucson, Arizona, USA, catalogue number 19348 and the RRUFF Project, deposition number R120109.

Description, occurrence, physical properties and mineral name

Marshallsussmanite forms bladed crystals with a pink colour (Figs 1 and 2). On the holotype specimen, marshallsussmanite is intense pink with a distinct orange tinge, grading towards a peach colour. Holotype marshallsussmanite has epitaxial serandite in association (Fig. 3), as well as minor later calcite

Fig. 1. The holotype specimen of marshallsussmanite, 9.5 cm across, showing pink bladed crystals to 1.3 cm with minor white calcite.

Fig. 2. A fine marshallsussmanite specimen from the Wessels mine, 9.1 cm tall. Weinrich Minerals specimen. Jeff Scovil photograph.

(Fig. 1). Another assemblage of marshallsussmanite is also known, associated with euhedral black prismatic aegirine, translucent white hydroxyapophyllite-(K) crystals and epitaxial pectolite overgrowths. These marshallsussmanite specimens are paler in colour and lack the orange tinge of holotype material, and possibly represent a separate find of the mineral. The lustre of marshallsussmanite is vitreous; crystals vary from transparent to translucent. The maximal crystal size observed in this study is 2.1 cm × 1.5 cm. The bladed crystals are elongated most along [010], typically with an aspect ratio of 3:2, and generally sit on matrix on their long edge.

Marshallsussmanite has a Mohs hardness of 5. The mineral shows perfect cleavage in two directions, {100} and {001}.
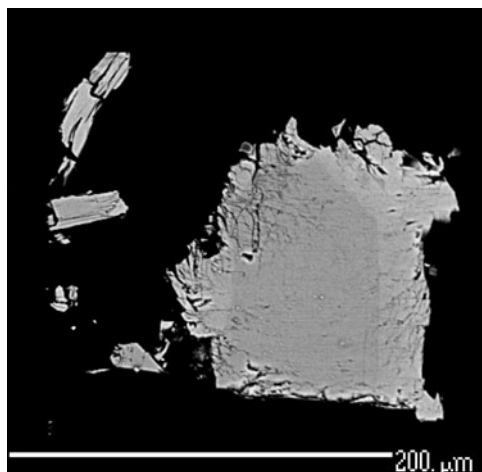
Fig. 3. Back-scattered electron photomicrograph of a zoned marshallsussmanite–serandite crystal, the brighter rim (right side of image) representing epitaxial serandite grown on darker marshallsussmanite.

Fracture normal to the cleavage planes is difficult to achieve, and marshallsussmanite splinters upon crushing.

Marshallsussmanite forms on dark grey-brown skarn, consisting primarily of quartz stained by iron and manganese oxide phases, in the Wessels mine at Black Rock, Northern Cape Province, South Africa. The Wessels mine lies within the economically significant Kalahari Manganese Field; collectively, the Wessels mine and the adjacent N'Chwaning mines are type locality to 25 mineral species at the time of writing (http://www.mindat.org). Marshallsussmanite probably formed via metasomatic alteration of manganese rich metasediments, within the temperature range 270–420°C and the pressure range 0.2–1.0 kbar (Gutzmer and Beukes, 1996).

The mineral name honours Marshall I. Sussman (1944–). Mr. Sussman is a lifelong collector of minerals. Mr. Sussman periodically visits southern Africa to acquire mineral specimens. On one such visit in 2011, Mr. Sussman returned to Arizona with a finely crystallized pink-peach mineral. The initial powder X-ray diffraction study showed similarities to ferrobustamite. Noting the pink colour and occurrence in the Kalahari Manganese Field, Mr. Sussman suspected significant manganese in the mineral. He brought the material to the attention of one of the authors (MJO) who then used single-crystal methods at the University of Arizona and found a triclinic unit cell intermediate to those of pectolite and serandite (Table 1). An independent powder X-ray diffraction study at the Smithsonian also showed the material to be isomorphous with pectolite. Further independent study using scanning electron microscopy with energy dispersive spectroscopy (SEM-EDS) at the Smithsonian Institution indicated

significant Na, Ca and Mn. A careful reading of Ohashi and Finger (1978) gave an inkling that this material represents a novel ordered intermediate $NaCaMnSi_3O_8OH$ compositionally midway between pectolite and serandite, and henceforth came this study.

Additional localities for marshallsussmanite exist. Notably, sample SCH of Ohashi and Finger (1978) corresponds to marshallsussmanite; it occurs in sodalite-syenite pegmatite at Kangerdlaursak, Julianehaab, Greenland. Carr et al. (1976) report 'manganoan pectolite' and 'calcian serandite' in phonolite from Mount Goonneringerringgi, Queensland, Australia; both minerals fall into the marshallsussmanite compositional field. Marshallsussmanite also occurs in the Aris phonolite, Windhoek, Namibia (Kolitsch et al., 2016). Type serandite analysed in Lacroix (1931) also falls into the marshallsussmanite composition field.

Chemical analysis and chemical formula

Chemical analyses were performed on a Cameca SX-100 electron microprobe housed in the Lunar and Planetary Laboratory at the University of Arizona. Wavelength dispersive spectroscopy scanning revealed Na, Ca, Si, Mn and minor Mg, but no other elements with $Z > 8$; notably no significant Fe was found. Operating conditions were 20 nA and 20 kV, with an estimated spot size <1 μm. Standards included albite (Na), forsterite (Mg), orthoclase (Si), wollastonite (Ca) and rhodonite (Mn). Table 2 includes the results of 20 microprobe spot analyses. Data reduction and corrections followed the 'PAP' methodology (Pouchou and Pichoir, 1984).

Back-scattered electron microscopy revealed chemical zonation in the material. Chemical analysis showed a clear distinction between a rather homogeneous marshallsussmanite zone with Ca: Mn ≈ 0.9:1.1 and a homogenous epitaxial serandite zone with Ca: Mn ≈ 0.1:1.9 (Fig. 3). Such zonation could represent exsolution of serandite from marshallsussmanite, or later deposition of serandite onto marshallsussmanite.

To quantify a suspected Li content, 4.2 mg of marshallsussmanite were digested in mixed concentrated hydrofluoric and nitric acids, re-precipitated by evaporation, and finally redissolved in 2% nitric acid. The sample solution was analysed with a Thermo Scientific XSeries II ICP-MS (Quadrupole Inductively Coupled Plasma Mass Spectrometer). Signal optimization employed a Thermo Fisher Scientific Multi-Element Tune A solution. A 1 ppm standard solution was made from stock solutions of 1000 ppm standards. Recursive tenfold dilutions were used to make internal standard solutions to 0.1 ppb. These diluted solutions were used to generate a calibration curve with a correlation coefficient of 0.9999, and ensured that both the pulse counting and the analogue detectors were operating synchronously. A BCR-2 standard was used during data reduction to calculate the Li concentration; estimated errors for Li are ±5%.

Table 1. Minerals of the pectolite group*.

		a (Å)	b (Å)	c (Å)	α (°)	β (°)	γ (°)	V (Å³)	Original description
Barrydawsonite-(Y)	$Na_{1.5}Y_{0.5}CaSi_3O_8(OH)$	15.5026	7.0233	6.9769	90	95.149	90	756.58	Mitchell et al. (2015)
Cascandite	$\square CaScSi_3O_8(OH)$	7.503	7.076	6.777	92.23	93.58	104.49	347.12	Mellini et al. (1982)
Marshallsussmanite	$NaCaMnSi_3O_8(OH)$	7.7854	6.9374	6.8516	90.683	94.330	102.856	359.59	this study
Pectolite	$NaCaCaSi_3O_8(OH)$	7.988	7.040	7.025	90.52	95.18	102.47	383.98	von Kobell (1828)
Serandite	$NaMnMnSi_3O_8(OH)$	7.7185	6.9064	6.7624	90.492	94.085	102.775	350.56	Lacroix (1931)
Tanohataite	$LiMnMnSi_3O_8(OH)$	7.612	7.038	6.700	90.23	94.70	105.26	345.0	Nagase et al. (2012)

*Cascandite, pectolite and serandite unit cell parameters from Mellini and Merlino (1982), Prewitt (1967) and Jacobsen et al. (2000), respectively.

Table 2. Empirical chemistry of marshallsussmanite*.

	Range	Average (s.d.) $n = 20$	Ideal
SiO_2	51.29–52.02	51.71(19)	51.91
MnO	21.13–22.24	21.79(34)	20.43
MgO	0.04–0.13	0.08(3)	
CaO	14.95–15.87	15.33(28)	16.15
Na_2O	7.34–8.43	8.06(35)	8.92
Li_2O	0.42–0.43	0.43(1)	
H_2O	n.d.	n.d.	2.59
Total		97.40	100.00

*Oxide values (Na,Mg,Ca,Mn,Si) from EPMA and Li values from ICPMS. Normalized to 3 Si atoms and assuming 1 H per formula unit, the empirical formula is $Li_{0.100}Na_{0.906}Ca_{0.953}Mg_{0.007}Mn_{1.071}Si_3O_8(OH)$.

Reduction of the electron microprobe analytical data showed a low metal to Si ratio, i.e. $\sum(Mn + Ca + Na + Mg) : Si$ of 2.937 : 3. In the refinement of the crystal structure of marshallsussmanite, free variation of the A-site occupancy yielded an electron density peak too low for a single Na atom, suggesting either a vacancy or presence of an element with $Z < 8$. Analysis using ICP-MS found significant Li in the mineral corresponding to 0.10 Li per formula unit. And crystal-structure refinement indicated the presence of 1 H apfu. The empirical formula for holotype marshallsussmanite, based on electron microprobe and ICP-MS data, calculated for 9 O atoms (and assuming 1 H apfu) is $Li_{0.100}Na_{0.906}Ca_{0.953}Mg_{0.007}Mn_{1.071}Si_3O_8(OH)$.

Crystallographic study

Powder X-ray diffraction

Powder X-ray diffraction data were collected on a Bruker D8 diffractometer, generating Cu$K\alpha$ radiation at 40 kV and 40 mA from a conventional sealed X-ray tube, filtered with Ni, and monochromated by a graphite crystal. The powder X-ray diffraction data were collected with step scans over 2θ range 5–90°, with step size 0.01° in 2θ and step count time of 2 s. Table 3 includes the powder diffraction data. Minor admixture with serandite (Fig. 3) caused minor peak broadening, precluding precise

Table 3. Powder X-ray diffraction data for marshallsussmanite.

I/I_0	d_{obs}	hkl
5	7.63	(100)
10	6.91	(001)
8	3.808	(200)
10	3.437	(002)
45	3.227	($\bar{1}$02),(201)
15	3.104	(0$\bar{1}$2)
100	3.041	(102),(012)
10	2.998	($\bar{1}$12)
20	2.868*	($\bar{2}$20),(120)
15	2.657	($\bar{2}$02)
20	2.534	(300)
8	2.288	($\bar{3}$20)
25	2.202	($\bar{1}$03)
5	2.121	(3$\bar{2}$1),(221)
15	1.715	($\bar{1}$40)
3	1.685	($\bar{3}\bar{2}$2)
3	1.642	($\bar{4}$22)
5	1.458	(501)
3	1.435	(124)

*broad

refinement of the unit-cell parameters of marshallsussmanite from the powder data.

Single-crystal X-ray diffraction

Thermal shocking of marshallsussmanite splinters with liquid nitrogen produced a few equidimensional crystal fragments. A cuboid of 50 μm × 40 μm × 40 μm was selected and mounted for diffraction study. Single-crystal X-ray diffraction was performed using a Bruker Apex II diffractometer housed at the Department of Geosciences, University of Arizona. The X-ray source is a fine focus sealed tube with a Mo target, operated at 50 kV and 30 mA, and collimated with multilayer X-ray optics.

A hemisphere of intensity data was collected (Table 4). The unit-cell dimensions were refined from the positions of 3558 observed reflections with I > 2σ over 2θ range 5.38–68.62°. The crystal intensity data were analysed with *Apex* software, integrated with Bruker *SAINT*, and reduced with *XPREP*. The crystal structure analysis initially used direct methods in *SHELXS* (Sheldrick, 2008) and subsequent refinement cycles utilized *SHELXL* (Sheldrick, 2008). The cation occupancies for the A (Na, Li), M1 (Ca, Mn) and M2 (Mn, Ca) sites were allowed to vary, each constrained to full occupancy. The H atom was located within a difference-Fourier map, and its position and its isotropic displacement parameter converged without restraint. Final atom coordinates are listed in Table 5 and selected geometric details appear in Table 6. A crystallographic information file and structure factor data have been deposited with the Principal Editor of *Mineralogical Magazine* and are available as supplementary material (see below). The structure is illustrated in Fig. 4.

Crystal structure

The crystal structure of marshallsussmanite consists of single chains of corner linked SiO_4 tetrahedra running along [010], connected by double ribbons of edge-sharing CaO_6 and MnO_6 octahedra also along [010], alongside a ribbon of irregular Na sites

Table 4. Marshallsussmanite crystal data and structure refinement details.

Crystal details	
size (μm)	50 × 40 × 40
colour	colourless with pink tinge
symmetry	P$\bar{1}$
a	7.7854(4) Å
b	6.9374(4) Å
c	6.8516(3) Å
α	90.683(3)°
β	94.330(3)°
γ	102.856(3)°
V	359.59(3) Å^3
Refinement details	
total reflections	2611
observed reflections	2189 with $I > 2\sigma(I)$
refined chemistry	$(Na_{0.948}Li_{0.052})(Ca_{0.793}Mn_{0.207})(Mn_{0.937}Ca_{0.063})Si_3O_8(OH)$
refined parameters	143
2–theta range	5–66°
h,k,l ranges	$-11 < h < 11$, $-10 < k < 10$, $0 < l < 10$
$R_{observed}$	0.0248
R_{all}	0.0351
wR_{all}	0.0620
Goof	1.054
weighting scheme	$w = 1/[\sigma^2(F_o^2) + (0.0291P)^2 + 0.2731P]$ where $P = (F_o^2 + 2F_c^2)/3$

Table 5. Fractional coordinates and displacement parameters for marshallsussmanite*.

	x/a	y/b	z/c	$U_{iso}*/U_{eq}$	U^{11}	U^{22}	U^{33}	U^{12}	U^{13}	U^{23}
A	0.55628 (11)	0.24615 (14)	0.35008 (13)	0.0166(3)	0.0105(4)	0.0196(5)	0.0181(4)	−0.0001(3)	0.0024(3)	−0.0003(3)
M1	0.84971 (4)	0.59370 (5)	0.14331 (5)	0.01032(9)	0.0107(2)	0.0096(2)	0.0106(2)	0.0021(1)	0.0006(1)	0.0003(1)
M2	0.85161 (4)	0.08466 (4)	0.13417 (4)	0.00975(8)	0.0094(1)	0.0097(2)	0.0101(1)	0.0025(1)	0.00005(9)	0.00001(9)
Si1	0.21937 (6)	0.40643 (8)	0.33658 (7)	0.0079(1)	0.0085(2)	0.0069(2)	0.0079(2)	0.0018(2)	−0.0011(2)	−0.0001(2)
Si2	0.20617 (6)	0.95897 (8)	0.35047 (7)	0.0079(1)	0.0084(2)	0.0073(2)	0.0078(2)	0.0017(2)	−0.0004(2)	−0.0001(2)
Si3	0.45193 (6)	0.74575 (8)	0.14240 (7)	0.0078(1)	0.0067(2)	0.0084(2)	0.0079(2)	0.0012(2)	−0.0005(2)	−0.0001(2)
O1	0.6592 (2)	0.8057 (2)	0.1190 (2)	0.0124(3)	0.0083(5)	0.0132(7)	0.0148(6)	0.0004(5)	0.0013(4)	0.0005(5)
O2	0.3247 (2)	0.7217 (2)	0.9432 (2)	0.0119(3)	0.0116(6)	0.0144(7)	0.0093(5)	0.0035(5)	−0.0029(4)	−0.0012(5)
O3	0.8099 (2)	0.4915 (2)	0.4586 (2)	0.0126(3)	0.0166(6)	0.0113(7)	0.0106(5)	0.0052(5)	−0.0008(5)	−0.0022(5)
O4	0.1551 (2)	0.8519 (2)	0.5517 (2)	0.0119(2)	0.0173(6)	0.0092(7)	0.0089(5)	0.0024(5)	0.0018(5)	0.0009(5)
O5	0.0603 (2)	0.3857 (2)	0.1706 (2)	0.0106(2)	0.0102(5)	0.0113(7)	0.0099(5)	0.0024(5)	−0.0016(4)	0.0001(5)
O6	0.0557 (2)	0.9025 (2)	0.1728 (2)	0.0108(2)	0.0096(5)	0.0129(7)	0.0097(5)	0.0029(5)	−0.0015(4)	−0.0012(5)
O7	0.4054 (2)	0.5330 (2)	0.2581 (2)	0.0132(3)	0.0106(5)	0.0112(7)	0.0175(6)	0.0016(5)	0.0015(5)	0.0042(5)
O8	0.3926 (2)	0.9046 (2)	0.2928 (2)	0.0112(3)	0.0095(5)	0.0115(7)	0.0128(6)	0.0036(5)	−0.0001(4)	−0.0025(5)
O9	0.2649 (2)	0.1960 (2)	0.3936 (2)	0.0106(2)	0.0117(6)	0.0078(6)	0.0120(6)	0.0019(5)	−0.0007(4)	0.0007(5)
H	0.153 (7)	0.688 (8)	0.563 (9)	0.13(2)*						

*Refined occupancies with errors: A = $Na_{0.948(5)}Li_{0.052(5)}$; M1 = $Ca_{0.793(6)}Mn_{0.207(6)}$; M2 = $Mn_{0.937(6)}Ca_{0.063(6)}$

(Fig. 4*a*). Alternatively, the marshallsussmanite structure may be considered layered with separate octahedral and tetrahedral layers (Fig 4*b*). Marshallsussmanite is isostructural with other members of the pectolite group (Table 1). Using the site nomenclature of Ohashi and Finger (1978), the marshallsussmanite crystal structure has Na in the A site, Ca in the M1 site and Mn in the M2 site. Sample SCH of Ohashi and Finger (1978) corresponds to marshallsussmanite, containing 64% of the ideal marshallsussmanite component. Holotype marshallsussmanite has refined chemistry $(Na_{0.948}Li_{0.052})(Ca_{0.793}Mn_{0.207})(Mn_{0.937}Ca_{0.063})Si_3O_8(OH)$, corresponding to 79% of the idealized end-member

$NaCaMnSi_3O_8(OH)$, with minor $LiNa_{-1}$, $MnCa_{-1}$ and $CaMn_{-1}$ substitutions.

The A site (Na) is an irregular coordination polyhedron of 7 O atoms within a radius of 3 Å. The A site bond-valence sum for all seven Na–O contacts gives too large of a sum (1.32 e^-). In order to analyse the bonding environment, a procrystal electron density distribution was generated by superimposing spherically averaged Roothan-Hartree-Fock wave functions (Downs *et al.*, 1996) onto the atomic positions of the marshallsussmanite crystal structure. In the procrystal electron density model, two Bader (1990) criteria were sought between Na and each nearby O with a cutoff distance

Table 6. Atomic separations and geometries for marshallsussmanite*.

A–O9	2.261(2) Å	Si1–O5	1.5975(13) Å
A–O2	2.268(2) Å	Si1–O3	1.6180(14) Å
A–O3	2.367(2) Å	Si1–O9	1.6222(14) Å
A–O8	2.440(2) Å	Si1–O7	1.6492(14) Å
<R(A–O)>	2.234(2) Å	<R(Si1–O)>	1.6218(14) Å
A···O4	2.536(2) Å	V(Si1O₄)	2.174 Å³
A···O7	2.588(2) Å	a.v.	20.63
A···O8	2.709(2) Å	q.e.	1.0048
M1–O3	2.3034(14) Å	Si2–O6	1.6054(14) Å
M1–O5	2.3083(13) Å	Si2–O4	1.6085(15) Å
M1–O1	2.3085(14) Å	Si2–O9	1.6231(15) Å
M1–O2	2.3469(15) Å	Si2–O8	1.6527(14) Å
M1–O6	2.3694(14) Å	<R(Si2–O)>	1.6224(15) Å
M1–O5	2.4120(14) Å	V(Si2O₄)	2.178 Å³
<R(M1–O)>	2.3414(14) Å	a.v.	17.68
V(M1O₆)	16.294 Å³	q.e.	1.0042
a.v.	118.14		
q.e.	1.0336	Si3–O1	1.5952(14) Å
		Si3–O2	1.6089(13) Å
M2–O1	2.1638(14) Å	Si3–O8	1.6615(14) Å
M2–O2	2.1677(14) Å	Si3–O7	1.6648(15) Å
M2–O4	2.1983(13) Å	<R(Si3–O)>	1.6326(14) Å
M2–O6	2.2426(13) Å	V(Si3O₄)	2.221 Å³
M2–O6	2.2709(13) Å	a.v.	17.71
M2–O5	2.3409(14) Å	q.e.	1.0040
<R(M2–O)>	2.2307(14)		
V(M2O₆)	14.421 Å³	O3···H	1.351 Å
a.v.	59.09	O4–H	1.136 Å
q.e.	1.0182	R(O3···O4)	2.458 Å
		angle(O3···H–O4)	162.7°

*Angle variance (a.v.) and quadratic elongation (q.e.) parameters defined by Robinson *et al.* (1971).
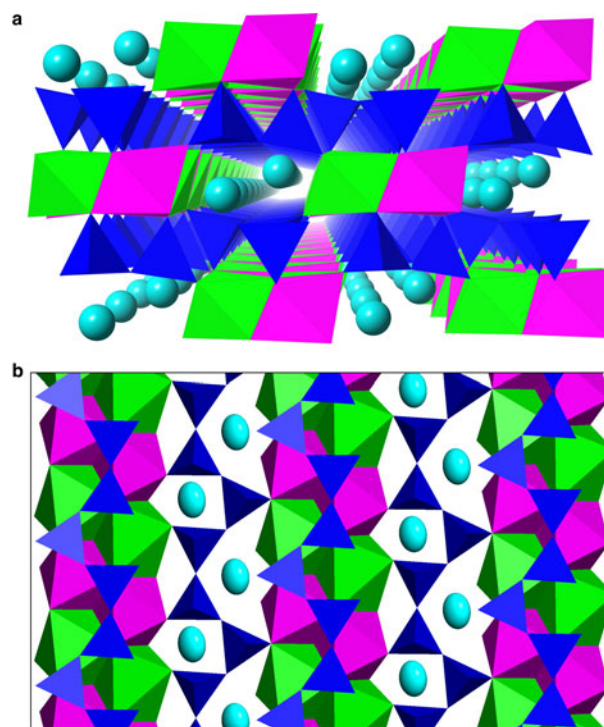

Fig. 4. The marshallsussmanite crystal structure: (*a*) perspective view along [010]; (*b*) a tetrahedral layer and an octahedral layer viewed down face pole (101), shown as cyan Na atoms, green CaO_6 octahedra, magenta MnO_6 octahedra and dark blue SiO_4 tetrahedra.

Table 7. Bond-valence sums for marshallsussmanite*.

	Na	Ca	Mn	Si1	Si2	Si3	Σ
O1		0.37	0.38			1.08	1.83
O2	0.28	0.33	0.37			1.04	2.02
O3	0.22	0.37		1.02			1.61
O4			0.34		1.04		1.38
O5		0.37	0.23	1.07			1.95
		0.28					
O6		0.31	0.31			1.05	1.95
			0.28				
O7				0.93		0.90	1.83
O8	0.18				0.93	0.90	2.01
O9	0.29			1.01	1.00		2.30
Σ	0.97	2.03	1.91	4.03	4.03	3.92	

*Calculations based on refined chemistry and parameters from Brese and O'Keeffe (1991) and Brown and Altermatt (1985). The low sums for O4 and O3 are consistent with an H atom position between O3 and O4, located nearer to O4.

of 5 Å. First a bond path is sought, which is a continuous path of local maxima of electron density between the two atoms; and second, a bond critical point along the bond path is sought, which is a $(3,\bar{1})$ saddle in electron density. The modelling software demonstrated four bonded interactions, specifically to the O2, O3, O4 and O9 atoms. For these bonded interactions, $<R(Na–O)> = 2.234(2)$ Å (Table 6). The bond-valence sum of these four interactions is $0.97\ e^-$ (Table 7), in good agreement with the expected valence for Na. The A site, with the Na displacement ellipsoid within a cage of 7 O atoms, including its four bonded interactions is shown in Fig. 5. Ostensibly, the displacement ellipsoid shows its greatest amplitude normal to these four interactions. The crystal structure refinement yielded an A-site scattering factor of $10.56\ e^-$, significantly less than $11\ e^-$ expected for atomic Na. Assuming full occupancy and the presence of Li in the A site, the site occupancy refined to $[Na_{0.948}Li_{0.052}]$.

The M1 (Ca) site in the marshallsussmanite structure has octahedral coordination with $<R(M1–O)> = 2.341$ Å and $V(M1O_6) = 16.29$ Å^3 (Table 6). The quadratic elongation (Robinson *et al.*, 1971) of $M1O_6$ is 1.0336, which indicates a rather distorted site. The refined occupancy of M1 is $[Ca_{0.793}Mn_{0.207}]$. The mean
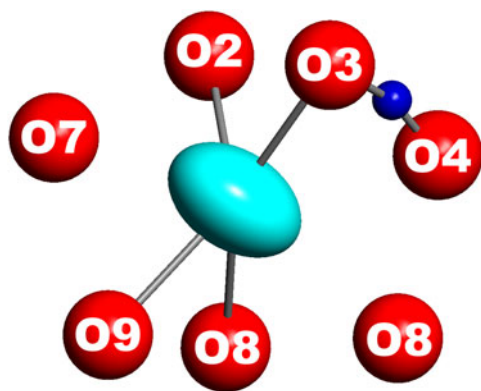

Fig. 5. The bonding environment of the A site in marshallsussmanite viewed along [011]. Procrystal electron density modelling indicates bond paths and critical points between Na and each of O2, O3, O8 and O9. These four interactions have a bond valence sum of $0.97\ e^-$. The long axis of the displacement ellipsoid lies roughly normal to these bonded interactions. Thus, the A-site with refined chemistry $[Na_{0.948(5)}Li_{0.052(5)}]$ in marshallsussmanite is 4-coordinate with $<R(Na–O)> = 2.234(2)$ Å.

bond length corresponds well with $<R(Ca1–O)> = 2.327$ Å for an octahedral site in pectolite with occupancy $[Ca_{0.73}Mn_{0.27}]$ (Arakcheeva *et al.*, 2007).

The M2 (Mn) site in the marshallsussmanite structure has octahedral coordination, and is a bit smaller and more regular than M1. Type marshallsussmanite has $<R(M2–O)> = 2.231$ Å, which compares favourably with $<R(Mn–O)>$ for two separate sites in serandite (Jacobsen *et al.*, 2000), with $<R(Mn–O)> = 2.261$ Å and $<R(Mn–O)> = 2.361$ Å. The two unique MnO_6 octahedra in serandite have $V = 14.81$ Å^3 and 14.36 Å^3. In marshallsussmanite, $V(M2O_6) = 14.42$ Å^3, with a refined M2 site occupancy of $[Mn_{0.937}Ca_{0.063}]$. The MnO_6 octahedron in natural johannsenite (Capitani and Mellini, 2000) has $<R(Mn–O)> = 2.164$ and $V = 13.42$ Å^3. Compared to johannsenite, the greater $<R(Mn–O)>$ in marshallsussmanite is consistent with minor Ca substitution. The quadratic elongation (Robinson *et al.*, 1971) of $M2O_6$ is 1.0182, which shows significantly less distortion than $M1O_6$.

There are three unique Si sites in marshallsussmanite: Si1, Si2, Si3. Each Si atoms shows tetrahedral coordination with O, with typical silicate bond distances (Table 6). Quadratic elongation and angle variance parameters (Robinson *et al.*, 1971) indicate these silicate tetrahedra are quite regular. Each SiO_4 groups shows rigid body behaviour (Downs, 2000), indicating complete cation ordering. Bond-valence sums for each of the Si atoms approach 4 (Table 7).

In pyroxenes, a repeat period of two silicate tetrahedra leads to the definition of a single chain angle ($\angle$O3–O3–O3). However, as marshallsussmanite has three distinct bridging O atoms (O7, O8, O9), there are three different chain angles $\angle$O7–O8–O9 = 155.95°; $\angle$O9–O7–O8 = 139.77°; $\angle$O8–O9–O7 = 116.25°. The mean bridging oxygen angle $<\angle$O–O–O$> = 137.32°$ (Fig. 6), corresponding to a highly compressed silicate chain (Thompson and Downs, 2004), in contrast to a fully extended chain with $<\angle$O–O–O$> = 180°$. The presence of a strong hydrogen bond between two non-bridging O atoms (O3 and O4) contributes to significant compression of the silicate chain (Fig. 7).

A hydrogen atom was located within the difference-Fourier maps; its positional and isotropic displacement parameters converged without restraint. The hydrogen atom is located between non-bridging O3 and O4 atoms in the silicate chain, which have a separation of 2.458(2) Å. Bond valence calculations (Table 7) indicate sums of $1.38\ e^-$ and $1.61\ e^-$ for O4 and O3, respectively. As O4 is less saturated than O3, H is expected nearer O4, as corroborated by the crystal structure refinement (Table 6).

Spectroscopic study

Raman spectra were collected on a Nicolet Almega microRaman spectrometer. Sample excitation wavelengths of 532 nm and 780 nm were used. The Raman spectra were collected with a 1800 lines cm^{-1} grating with an average resolution of 2.1 pixels/cm^{-1}. Marshallsussmanite spectra collected with 532 nm excitation showed moderate fluorescence whereas spectra collected at 780 nm excitation had low backgrounds with excellent signal-to-noise ratios. Figure 8 compares the Raman spectra of marshallsussmanite at 780 nm (R120109) with pectolite at 532 nm (R050396) and serandite at 532 nm (R040056). Complete spectral data are available from the RRUFF database (Lafuente *et al.*, 2015).

The most prominent feature of the Raman spectrum of marshallsussmanite is an Si–O–Si bending mode at 659 rel. cm^{-1} (Fig. 8a). The Raman spectrum is similar to those of isostructural

pectolite

$NaCaCaSi_3O_8(OH)$

Prewitt (1967)

marshallsussmanite

$NaCaMnSi_3O_8(OH)$

this study

serandite

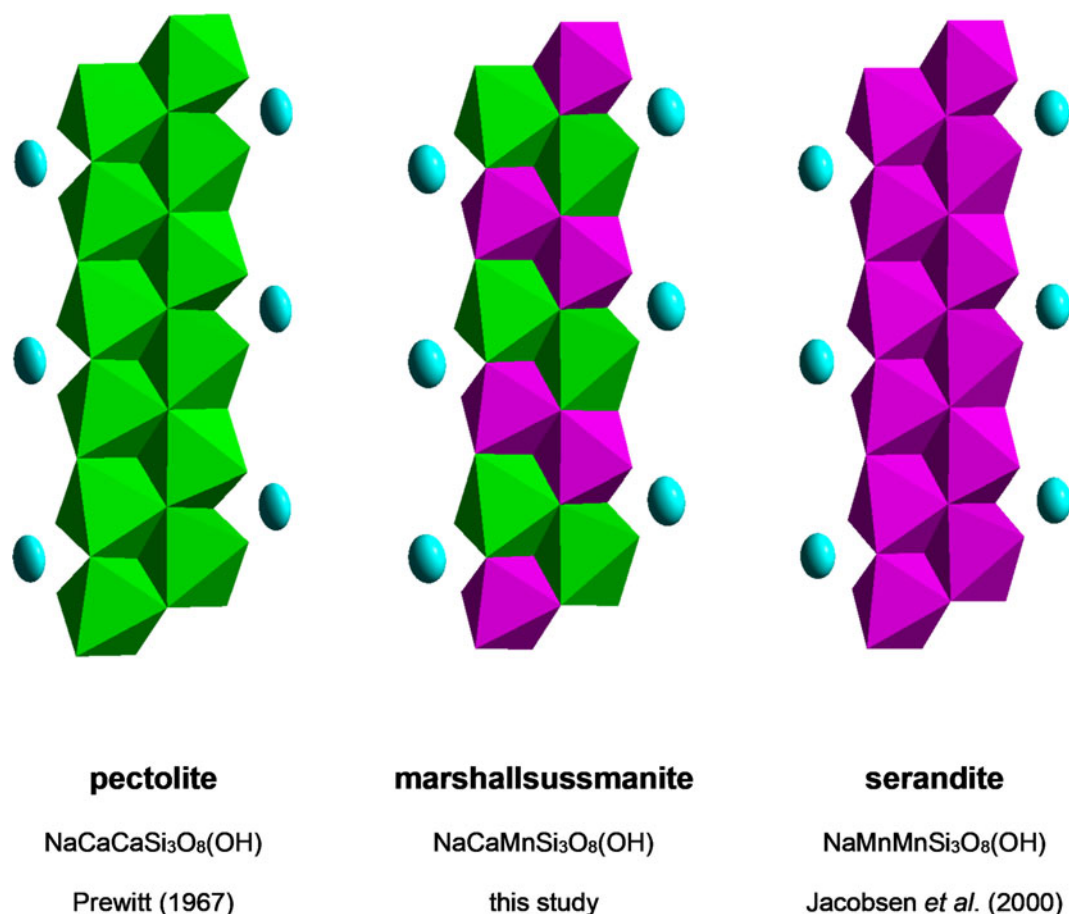$NaMnMnSi_3O_8(OH)$

Jacobsen *et al.* (2000)

Fig. 6. Comparison of the cation ribbons viewed along face pole (101) of the pectolite, marshallsussmanite and serandite crystal structures. Atoms shown as cyan Na ellipsoids, green CaO_6 octahedra and magenta MnO_6 octahedra.

pectolite and serandite. The peak at 1010 rel. cm^{-1} corresponds to a stretching of non-bridging Si–O bonds. Peaks in the 200–400 rel. cm^{-1} range relate to rotational modes and bending modes of the octahedral cations. The H-bond stretching modes for marshallsussmanite, pectolite and serandite in the frequency range (1370–1390 rel. cm^{-1}) are shown in Fig. 8*b*, which are consistent with short $d(H\cdots O) \approx 1.4$–1.6 Å separations (Libowitzky, 1999).

Distinguishing marshallsussmanite, pectolite and serandite

Marshallsussmanite has properties similar to both pectolite and serandite. However, despite similarities in their powder X-ray diffraction profiles, unit-cell refinement to four significant figures can reliably distinguish these species (Table 1). Single-crystal methods can reliably distinguish these species. Standardized chemical analysis also affords reliable discrimination of pectolite-group species, and in many cases, semi-quantitative SEM-EDS analysis is sufficient. Raman spectroscopy also distinguishes the species; for instance, a prominent Si–O–Si bending mode occurs at 667 rel. cm^{-1} in serandite, 650 rel. cm^{-1} in pectolite and 659 rel. cm^{-1} in marshallsussmanite (Fig. 8).

Discussion

The pectolite–marshallsussmanite–serandite solid solution series exhibits significant ordering tendencies between Ca and Mn.

The structure type includes two separate octahedral M sites with $V(M1O_6) > V(M2O_6)$. The M1 site shows a strong preference for Ca (Takéuchi *et al.*, 1976, Ohashi and Finger, 1978), while M2 shows a strong preference for Mn (Takéuchi and Kudoh, 1977; Arakcheeva *et al.*, 2007). Ohashi and Finger (1978) remarked on the stepwise solid solution between pectolite ($NaCa_2Si_3O_8OH$) and serandite ($NaMn_2Si_3O_8OH$), foretelling the intermediate ordered phase named herein marshallsussmanite ($NaCaMnSi_3O_8OH$).

Crystallographic ordering of Ca and Mn also occurs in various isomorphous minerals, especially in the Kalahari Manganese Field. The Kalahari Manganese Field is type locality to the isostructural pyroxenoids olmiite $CaMnSiO_3(OH)_2$ and poldervaartite $Ca(Ca,Mn)SiO_3(OH)_2$ (Bonazzi *et al.*, 2007, Dai *et al.*, 1993). Other isomorphous Ca-Mn minerals in the Kalahari Manganese Field include the olivines tephroite Mn_2SiO_4 and glaucochroite $CaMnSiO_4$ (Cairncross and Beukes, 2013), and the carbonates calcite, rhodochrosite and kutnahorite (Cairncross and Beukes, 2013). At sufficient temperature, Ca and Mn atoms disorder in the calcite-rhodochrosite structure (Peacor *et al.*, 1987), implying that kutnahorite $CaMn(CO_3)_2$ provides an upper bound temperature for mineral genesis. More generally, study of order-disorder relations of isomorphous Ca-Mn minerals in the Kalahari Manganese Field should provide further insight into deposit genesis.

Hydrous pyroxenoid structures, such as the isostructural *fünfer* chain species babingtonite, nambulite, natronambulite, marsturite
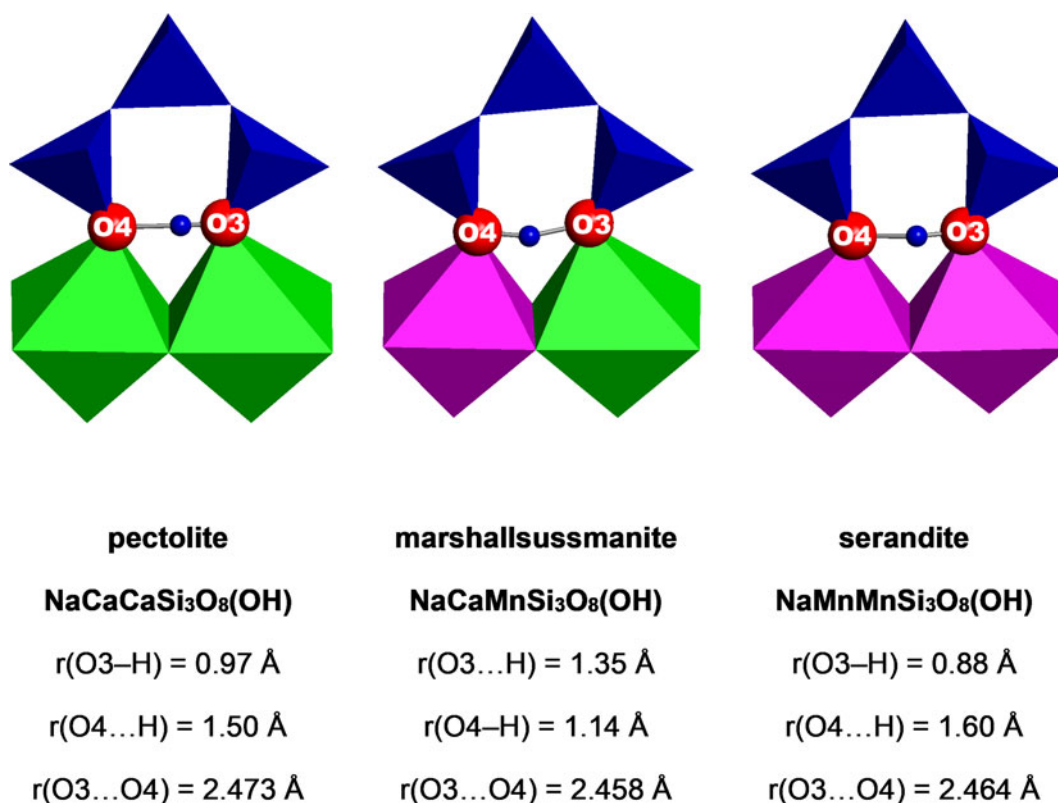
Fig. 7. The hydrogen bonding environments in the pectolite-group minerals, viewed along [413]. In marshallsussmanite, O4 acts as the donor atom, while in both pectolite and serandite, O3 acts as the donor atom. The H position acts a proxy for the relative saturation of the O3 and O4 atoms by nearby cations, in accord with bond-valence summations.

and lithiomarsturite exhibit very strong hydrogen bonds. The H bonds occur between non-bridging O atoms (O1 and O11) in the silicate chain. In nambulite, natronambulite, marsturite and lithiomarsturite, H atoms are located between non-bridging O1 and O11 atoms in the silicate chain. These minerals have O1···O11 separations of 2.460–2.472 Å (Nagashima *et al.*, 2014*a*; Yang *et al.*, 2011). Yang *et al.* (2011) argues that the H position in lithiomarsturite is a consequence of the relative saturation of the O1 and O11 atoms, specifically with O11 as the H-bond donor. In babingtonite which has O1···O11 separations of 2.563–2.571 Å (Nagashima *et al.*, 2014*b*), O1 however acts as the H-bond donor and O11 as the acceptor. Liebau (1980) argues that electronegativity of the metal ions in the cation layers affects the H bonding environment. Nagashima *et al.* (2014*a*) show that the substitution of Li for Na lead to a shift in H position in the isostructural minerals marsturite, lithiomarsturite, nambulite and natronambulite. The explanation given is that Li and Na actually have slightly different positions in the structure, with Li shifted away from O11. In Li-dominant lithiomarsturite and nambulite, O11 is the H-bond donor and O1 is the acceptor; while in Na-dominant natronambulite and marsturite, the opposite is true.

Like the *fünfer* chain pyroxenoids, the *dreier* chain pectolite-group species (Table 1) exhibit very strong hydrogen bonds. The H-bonds link non-bridging O atoms in the silicate chain (O3 and O4). In pectolite (Prewitt, 1967), marshallsussmanite (this study) and serandite (Jacobsen *et al.*, 2000), the O3···O4 separations are 2.482 Å, 2.458(2) Å and 2.464(1) Å, respectively. In serandite (Jacobsen *et al.*, 2000) and pectolite (Prewitt, 1967), O3 acts as

the H-bond donor, with O4 as the H-bond acceptor. In marshallsussmanite however, the roles are switched: O4 is the H-bond donor and the O3 is the H-bond acceptor. Bond-valence sums for O3 in pectolite (Prewitt, 1967; Arakcheeva *et al.*, 2007) and serandite (Takéuchi *et al.*, 1976; Jacobsen *et al.*, 2000) both show less saturation for O3 than for O4, while the opposite case is seen in marshallsussmanite (Ohashi and Finger, 1978; this study). Not only does marshallsussmanite form an ordered intermediate between pectolite and serandite, it also switches its H-bonding scheme from that of pectolite and serandite. This reversal of H-bonding roles of O3 and O4 must relate to M1 and M2 site occupancies, as all three species have Na in the A site. Consequently, divalent cations (Ca, Mn) are as important as univalent cations (Na, Li) in these phases for determining the H position and H-bonding environment in pyroxenoids. Cation compositions near marshallsussmanite$_{2/3}$serandite$_{1/3}$ and marshallsussmanite$_{3/4}$pectolite$_{1/4}$ should exhibit symmetric H bonding by this model.

Arakcheeva *et al.* (2007) argued that the pectolite-type silicate chain consists of rigid HSi_3O_{10} units, similar in topology to the Si_4O_{12} units in the looped *dreier* chain in synthetic $Li_2Mg_2Si_4O_{11}$ (Czank and Bissert, 1993). Arakcheeva *et al.* (2007) further suggests that the cation layer geometries are determined by the rigidity of the silicate layer, and its periodicity caused by the intrachain H bond. Rigidity in the silicate layer would also manifest itself in the stability of vacancies in the cation layer, seen in the pectolite-group mineral cascandite $\square CaScSi_3O_8(OH)$ (Mellini and Merlino, 1982) and *fünfer* pyroxenoids babingtonite $\square Ca_2Fe^{2+}Fe^{3+}Si_5O_{14}(OH)$ and manganbabingtonite $\square Ca_2Mn^{2+}Fe^{3+}Si_5O_{14}(OH)$ (Nagashima
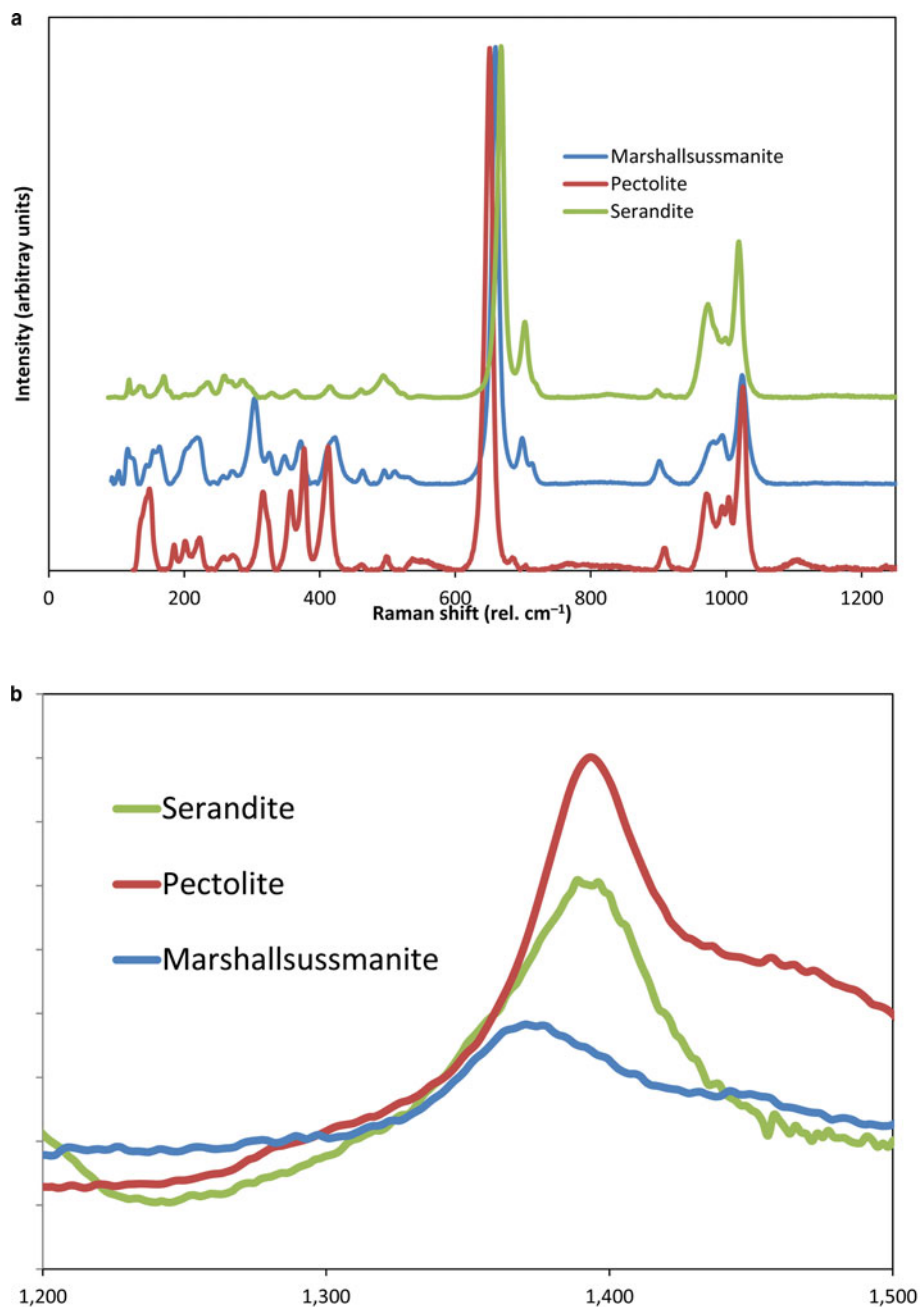
Fig. 8. (*a*) Raman spectra of R120109 marshallsussmanite, R050396 pectolite and R040056 serandite. Peak positions in these spectra have sufficient separation to permit identification solely by Raman spectroscopy. (*b*) Hydrogen bond stretching modes of R120109 marshallsussmanite, R050396 pectolite and R040056 serandite. The relatively strong H-bond stretching modes are expected for very short O3–O4 separations ~ 2.5 Å.

et al., 2014*b*). Many novel species are possible in the pectolite structure type, especially with vacant alkali sites, such as compositions like $CaM^{3+}Si_3O_9H$ or $Mn^{2+}M^{3+}Si_3O_9H$.

References

Arakcheeva, A., Pattison, P., Meisser, N., Chapuis, G., Pekov, I. and Thélin, P. (2007) New insight into the pectolite – serandite series: a single crystal diffraction study of $Na(Ca_{1.73}Mn_{0.27})[HSi_3O_9]$ at 293 and 100 K. *Zeitschrift für Kristallographie*, **222**, 696–704.

Bader, R.F.W. (1990) *Atoms in Molecules: A Quantum Theory*. Oxford University Press, UK, 458 pp.

Bonazzi, P., Bindi, L., Medenbach, O., Pagano, R., Lampronti, G.I. and Menchetti, S. (2007) Olmiite, $CaMn[SiO_3(OH)](OH)$, the Mn-dominant analogue of poldervaartite, a new mineral species from Kalahari manganese fields (Republic of South Africa). *Mineralogical Magazine*, **71**, 193–201.

Brese, N.E. and O'Keeffe, M.O. (1991) Bond-valence parameters for solids. *Acta Crystallographica*, **B47**, 192–197.

Brown, I.D. and Altermatt, D. (1985) Bond-valence parameters obtained from a systematic analysis of the Inorganic Crystal Structure Database. *Acta Crystallographica*, **B41**, 244–247.

Buerger, M.J. (1956) The determination of the crystal structure of pectolite, $Ca_2NaHSi_3O_9$. *Zeitschrift für Kristallographie*, **108**, 248–262.

Cairncross, B. and Beukes, N.J. (2013) *The Kalahari Manganese Field: The Adventure Continues*. Assore. Struik Nature, Cape Town, South Africa, 384 pp.

Capitani, G.C. and Mellini, M. (2000) The johannsenite-hedenbergite complete solid solution: clinopyroxenes from the Campiglia Marittima skarn. *European Journal of Mineralogy*, **12**, 1215–1227.

Carr, G.R., Phillips, E.R. and Williams, P.R. (1976) An occurrence of eudialyte and manganoan pectolite in a phonolite dyke from south-eastern Queensland. *Mineralogical Magazine*, **40**, 853–856.

Chester, A.H. (1896) *A Dictionary of the Names of Minerals Including Their History and Etymology. First Edition.* John Wiley & Sons, New York, 320 pp.

Czank, M. and Bissert, G. (1993) The crystal structure of $Li_2Mg_2[Si_4O_{11}]$, a loop-branched dreier single chain silicate. *Zeitschrift für Kristallographie*, **204**, 129–142.

Dai, Y., Harlow, G.E. and McGhie, A.R. (1993) Poldervaartite, $Ca(Ca_{0.5}Mn_{0.5})$ $(SiO_3OH)(OH)$, a new acid nesosilicate from the Kalahari manganese field, South Africa: Crystal structure and description. *American Mineralogist*, **78**, 1082–1087.

Dana, E.S. (1892) *The System of Mineralogy. 6th Edition.* John Wiley & Sons, New York, 1134 pp.

Downs, R.T. (2000) Analysis of harmonic displacement factors. Pp. 61–88 in: *High-Temperature and High-Pressure Crystal Chemistry* (R.M. Hazen and R.T. Downs, editors). Reviews in Mineralogy & Geochemistry, **41**. Mineralogical Society of America and the Geochemical Society, Chantilly, Virginia, USA.

Downs, R.T., Andalman, A. and Hudacsko, M. (1996) The coordination numbers of Na and K atoms in low albite and microcline as determined from a procrystal electron-density distribution. *American Mineralogist*, **81**, 1344–1349.

Gutzmer, J. and Beukes, N.J. (1996) Mineral paragenesis of the Kalahari manganese field, South Africa. *Ore Geology Reviews*, **11**, 405–428.

Hintze, C. (1897) *Handbuch der Mineralogie. Zweiter Band. Silicate und Titanate.* Verlag von Veit & Comp., Leipzig, Germany, 1841 pp.

Jacobsen, S.D., Smyth, J.R., Swope, R.J. and Sheldon, R.I. (2000) Two proton positions in the very strong hydrogen bond of serandite, $NaMn_2[Si_3O_8(OH)]$. *American Mineralogist*, **85**, 745–752.

Kolitsch, U., Blass, G., Jahn, S., Cámara, F., Von Bezing, L., Wartha, R.R., Tremmel, G., Sturla, M., Cerea, P., Skebo, M. and Ciriotti, M.E. (2016) *Aris. Mineralogy of the Famous Alkaline Phonolite.* Associazione Micromineralogia Italiana, Cremona, Italy, 95 pp.

Lacroix, A. (1931) Les pegmatites de la syénite sodalitique de l'île Rouma (archipel de Los, Guinée française). Description d'un nouveau minéral (sérandite) qu'elles renferment. *Comptes Rendus Hebdomadaires des Séances de l'Académie des Sciences*, **192**, 189–194.

Lafuente, B., Downs, R.T., Yang, H. and Stone, N. (2015) The power of databases: the RRUFF project. Pp. 1–30 in: *Highlights in Mineralogical Crystallography* (T. Armbruster and R.M. Danisi, editors). De Gruyter, Berlin, Germany.

Libowitzky, E. (1999) Correlation of O–H stretching frequencies and O–H⋯O hydrogen bond lengths in minerals. *Monatshefte fur Chemie*, **130**, 1047–1059.

Liebau, F. (1980) The role of cationic hydrogen in pyroxenoid crystal chemistry. *American Mineralogist*, **65**, 981–985.

Mellini, M. and Merlino, S. (1982) The crystal structure of cascandite, $CaScSi_3O_8(OH)$. *American Mineralogist*, **67**, 604–609.

Mellini, M., Merlino, S., Orlandi, P. and Rinaldi, R. (1982) Cascandite and jervisite, two new scandium silicates from Baveno, Italy. *American Mineralogist*, **67**, 599–603.

Mitchell, R.H., Welch, M.D., Kampf, A.R., Chakhmouradian, A.K. and Spratt, J. (2015) Barrydawsonite-(Y), $Na_{1.5}CaY_{0.5}Si_3O_9H$: a new pyroxenoid of the pectolite–serandite group. *Mineralogical Magazine*, **79**, 671–686.

Nagase, T., Hori, H., Kitamine, M., Nagashima, M., Abduriyim, A. and Kuribayashi, T. (2012) Tanohataite, $LiMn_2Si_3O_8(OH)$: a new mineral from the Tanohata mine, Iwate Prefecture, Japan. *Journal of Mineralogical and Petrological Sciences*, **107**, 149–154.

Nagashima, M., Armbruster, T., Kolitsch, U. and Pettke, T. (2014a) The relation between Li ↔ Na substitution in five-periodic single-chain silicates nambulite and marsturite: a single crystal X-ray study. *American Mineralogist*, **99**, 1462–1470.

Nagashima, M., Mitani, K. and Akasada, M. (2014b) Structural variation of babingtonite depending on cation distribution at the octahedral sites. *Mineralogy and Petrology*, **108**, 287–301.

Ohashi, Y. and Finger, L.W. (1978) The role of octahedral cations in pyroxenoid crystal chemistry. I. Bustamite, wollastonite, and the pectolite–schizolite–serandite series. *American Mineralogist*, **63**, 274–288.

Peacock, M.A. (1935) On pectolite. *Zeitschrift für Kristallographie*, **90**, 97–111.

Peacor, D.R., Essene, E.J. and Gaines, A.M. (1987) Petrologic and crystal-chemical implications of cation order-disorder in kutnahorite [CaMn $(CO_3)_2$]. *American Mineralogist*, **72**, 319–328.

Pouchou, J.L. and Pichoir, F. (1984) Un nouveau modèle de calcul pour la microanalyse quantitative par spectrométrie de rayons X. Partie I: Application a l'analyse d'énchantillons homogènes. *La Recherche Aérospatiale*, **3**, 167–192.

Prewitt, C.T. (1967) Refinement of the structure of pectolite, $Ca_2NaHSi_3O_9$. *Zeitschrift für Kristallographie*, **125**, 298–316.

Robinson, K., Gibbs, G.V. and Ribbe, P.H. (1971) Quadratic elongation: A quantitative measure of distortion in coordination polyhedra. *Science*, **172**, 567–570.

Schaller, W.T. (1955) The pectolite–schizolite–serandite series. *American Mineralogist*, **40**, 1022–1031.

Sheldrick, G.M. (2008) A short history of SHELX. *Acta Crystallographica*, **A64**, 112–122.

Takéuchi, Y. and Kudoh, Y. (1977) Hydrogen bonding and cation ordering in Magnet Cove pectolite. *Zeitschrift für Kristallographie*, **146**, 281–292.

Takéuchi, Y., Kudoh, Y. and Yamanaka, T. (1976) Crystal chemistry of the serandite–pectolite series and related minerals. *American Mineralogist*, **61**, 229–237.

Thompson, R.M. and Downs, R.T. (2004) Model pyroxenes II: Structural variation as a function of tetrahedral rotation. *American Mineralogist*, **89**, 614–628.

von Kobell, F. (1828) Ueber den Pektolith. *Archiv für die gesammte Naturlehre*, **13**, 385–393.

Warren, B.E. and Biscoe, J. (1931) The crystal structure of the monoclinic pyroxenes. *Zeitschrift für Kristallographie*, **80**, 391–401.

Williams, J.F. (1891) Manganopektolith, ein neues Pektolith-ähnliches Mineral von Magnet Cove, Arkansas. *Zeitschrift für Kristallographie*, **18**, 386–389.

Williams, E.R. and Weller, M.T. (2014) A variable-temperature neutron diffraction study of serandite: A Mn-silicate framework with a very strong, two-proton site, hydrogen bond. *American Mineralogist*, **99**, 1755–1760.

Winther, C. (1901) Schizolite, a new mineral. *Meddelelser om Grønland*, **24**, 196–203.

Yang, H., Downs, R.T. and Yang, Y.W. (2011) Lithiomarsturite, $LiCa_2Mn_2Si_5O_{14}(OH)$. *Acta Crystallographica*, **E67**, i73.